

Uptake, localization and dissolution of barium sulfate nanoparticles in human lung cells explored by the combination of ICP-MS, TEM and NanoSIMS

Maria Angels Subirana^a, Sarah Thomas^b, Gerd Hause^c, Dirk Dobritzsch^d, Felix Glahn^b, Dirk Schaumlöffel^{a,*}, Martin Herzberg^{e,1}

^a CNRS, Université de Pau et des Pays de l'Adour, E2S UPPA, Institut des Sciences Analytiques et de Physico-Chimie pour l'Environnement et les Matériaux (IPREM), UMR 5254, 64000 Pau, France

^b Martin-Luther-University Halle-Wittenberg, Institute of Environmental Toxicology, Franzosenweg 1a, 06097 Halle (Saale), Germany

^c Martin-Luther-University Halle-Wittenberg, Biozentrum, Weinbergweg 22, 06120 Halle (Saale), Germany

^d Martin-Luther-University Halle-Wittenberg, Core Facility – Proteomic Mass Spectrometry, Kurt-Mothes-Str. 3a, 06120 Halle (Saale), Germany

^e Martin-Luther-University Halle-Wittenberg, Institute for Biology / Microbiology, Kurt-Mothes-Str. 3, 06120 Halle (Saale), Germany

ARTICLE INFO

Keywords:

NanoSIMS

TEM

ICP-MS

Barium sulfate nanoparticles

Toxicity

Normal human bronchial epithelial cells

ABSTRACT

Background: Barium sulfate nanoparticles (BaSO₄-NPs) are considered to be poorly soluble, chemically inert, and therefore relatively non-toxic. For humans, inhalative exposure represents the most significant route of uptake. **Objective and methods:** Cellular effects after exposure to BaSO₄-NPs for 24 and 72 h have been investigated in this study on primary human lung cells. To track the fate of BaSO₄-NPs in human lung cells, we used inductively coupled plasma mass spectrometry (ICP-MS) to quantify cellular uptake of NPs, as well as transmission electron microscopy (TEM) and nanoscale secondary ion mass spectrometry (NanoSIMS) to investigate subcellular distribution of NPs through high-resolution elemental imaging.

Results and conclusions: We show that BaSO₄ nanoparticles have been taken up by normal human bronchial epithelial cells (NHBE) in a dose-dependent manner. However, no clear time-dependent uptake could be observed. The barium sulfate nanoparticles were visible in vesicles within the cytosol by TEM, which was confirmed by high-resolution NanoSIMS images. Nevertheless, no uptake of the particles into the nucleus was observed in this study. However, it was shown that BaSO₄-NPs were partly dissolved, and barium ions were distributed throughout the entire cell. Toxicity of the particles was indicated by a dose- and time-dependent loss of viability in human lung cells.

1. Introduction

Today, nanomaterials are used in a variety of industrial processes and thus they can enter the environment and under some circumstances even the food chains [1]. These nanomaterials, mostly produced from carbon or metals with diameters ranging of 1–100 nm, can consist of a mix of materials, and be coated with inorganic or organic compounds [2]. Toxicological evaluation of potentially hazardous properties of nanoparticles and associated health effects have been a major focus over the last two decades, with publications on nanoparticle toxicity rapidly increasing [3]. Metal nanoparticles such as titanium oxide, cerium

oxide, barium sulfate, silver, gold, platinum and alumina have been widely used for industrial purposes. Some of the toxicological effects of nanoparticles (NP) are related to their physical properties and some highly soluble NPs exhibit higher toxicity than poorly soluble NPs due to better absorption and increased ion release after oral or inhalation exposure [4].

Barium sulfate (BaSO₄) is a nanomaterial with a very low solubility. Its most significant properties include high density (4.5 g cm⁻³), chemical inertness, and reflectivity of electromagnetic radiation. BaSO₄ is considered a poorly soluble particle (PSP) or poorly soluble low toxicity (PSLT) due to its low solubility (2.2 mg L⁻¹, at 18 °C) [5]. Cerium

* Corresponding author.

E-mail address: dirk.schaumloeffel@univ-pau.fr (D. Schaumlöffel).

¹ present address: Helmholtz Centre for Environmental Research GmbH (UFZ), Department of Solar Materials Biotechnology (SOMA), Permoserstr. 15, 04318 Leipzig, Germany

<https://doi.org/10.1016/j.jtemb.2025.127650>

Received 4 December 2024; Received in revised form 27 February 2025; Accepted 8 April 2025

Available online 9 April 2025

0946-672X/© 2025 The Authors. Published by Elsevier GmbH. This is an open access article under the CC BY license (<http://creativecommons.org/licenses/by/4.0/>).

dioxide (CeO₂) and titanium dioxide (TiO₂) also belong to these categories [6]. Barium sulfate is almost insoluble in water, acids, and alkaline solutions, with the exception of hot, concentrated sulfuric acid. Due to these properties, it is often used as a color pigment or to enhance weathering resistance of paints. It is also used as a filler in the paper and plastics industries to improve smoothness and fire-resistance of paper [7], processability [8] and sound absorption of plastics. Additionally, BaSO₄ is used as a contrast agent in medical implants such as catheters or bone cement [9,10], improving antimicrobial properties, cytocompatibility with osteoblasts as well as radio-opacity [11,12].

Due to this extensive commercial use, the quantitative uptake and cellular fate of NPs is crucial for further toxicological assessment, even though these so-called biodegradable nanomaterials are assumed to be poorly absorbed from the gut or lungs into the blood [13]. BaSO₄-NPs introduced into the lungs of rats were shown to cause less injury and inflammation compared to CeO₂-NPs with similar size and dose based on number concentration [14,15]. However, particles of different sizes with the same composition can trigger different biological reactions [16]. Particle transport, distribution and deposition in the respiratory system depend on the structure of the lung, airflow characteristics, and particle properties such as size, shape and density [17].

Element-specific imaging can localize chemical elements, including metals and metal-containing nanoparticles, in biological tissues and cells, thus providing the potential to study the uptake and fate of nanoparticles at the cellular or even subcellular level [18]. Nanoscale secondary ion mass spectrometry (NanoSIMS) is an analytical technique using a primary ion beam to sputter the sample surface and which separates and detects the generated secondary ions in a mass spectrometer. A primary ion beam of cesium (Cs⁺) or oxygen (O⁻) scans the sample surface, producing elemental maps with resolutions down to 40–50 nm. Cesium ion sources are well established for producing negative secondary ions and mapping elements such as nitrogen, phosphorus and sulfur in biological samples. Recently, a bright RF plasma O⁻ primary ion source was implemented in NanoSIMS to generate positive secondary ions [19], capable of mapping metals and metal-containing nanoparticles in cells with a spatial resolution similar to the cesium source. Other chemical imaging techniques, such as laser ablation inductively coupled plasma mass spectrometry (LA-ICP-MS), typically provide probe sizes in the micron range but cannot achieve spatial resolution small enough for nanoparticle studies. Additionally, NanoSIMS offers high sensitivity compared to other imaging methods like transmission electron microscopy coupled with energy-dispersive X-ray spectroscopy (TEM/X-EDS). Therefore, NanoSIMS provides excellent lateral resolution and high sensitivity for element-specific nanoparticle analysis. However, for very small nanoparticles, the minimum beam size of approximately 40–50 nm may be similar to or even larger than the nanoparticle itself, potentially leading to an overestimation of the nanoparticle size [20]. Therefore, an additional TEM observation for NP size measurement is useful.

Combining TEM and NanoSIMS techniques is optimal for localizing nanoparticles within cells, tissues and organs. To date, only few nanoparticle studies have applied NanoSIMS and NanoSIMS/TEM, focusing on silver, titanium dioxide, silicon oxide, copper oxide, mercury selenide and gadolinium NP analysis [21]. However, barium sulfate nanoparticles have not been studied with NanoSIMS so far. Most studies used exclusively the Cs⁺ primary ion source for NP analysis, limiting investigations to elements (e.g., Ag, Ti, Si, and Cu) detectable in this ion source mode. For example, the uptake and fate of silver, titanium oxide and silicon oxide NPs were studied in *Daphnia magna* [22]. The environmental impact of silver nanoparticles has been studied through interactions with various aquatic organisms such as the green algae *Raphidocelis subcapitata* [23], the unicellular alga *Chlamydomonas reinhardtii* [24], the oyster larvae *Crassostrea angulata* [25] and the gill filaments of oysters [26], the gammarid *Gammarus fossarum* [27], the algae *Desmodesmus subspicatus*, the bacterium *Vibrio fischeri*, and the crustacean *Daphnia magna* [28]. The capacity of Ag-NPs to cross the

gastrointestinal epithelium was studied in vitro in a co-culture model with Caco-2/TC7:HT29-MTX intestinal cells [29]. Combining confocal imaging, synchrotron-based X-ray fluorescence (XRF) and NanoSIMS demonstrated that TiO₂-NPs could cross the gut barrier of rats [30]. Furthermore, NanoSIMS and TEM revealed that human HaCaT cells took up TiO₂-NPs through autophagosomes [31]. Another NanoSIMS study demonstrated the uptake of copper oxide NPs by human HepG2 cells [32]. Recently, mercury analysis by NanoSIMS was developed, which enabled localization of HgSe nanoparticles in the liver of sperm whales using both O⁻ and Cs⁺ primary ion sources [33]. Additionally, NanoSIMS (both ion source modes) combined with STEM-EDX and single-particle ICP-MS showed the accumulation gadolinium nanoparticles in deep cerebellar nuclei of rats [34]. A comprehensive overview of NanoSIMS for nanoparticle and nano-pollutant analysis was recently published by Subirana and Schaumlöffel [21].

In this study, we investigated the relative toxicity, quantitative uptake, and cellular distribution, as well as accumulation of BaSO₄-NPs in normal human bronchial epithelial cells (NHBE). The high-sensitivity and high-resolution imaging of macro and trace elements using NanoSIMS, equipped with a bright RF plasma O⁻ primary ion source and a conventional cesium ion source, enabled us to trace the fate of BaSO₄-NPs at cellular and subcellular levels. Thus, we were able to correlate the cell shape and structure determined by the subcellular distribution of macroelements with the fate of NPs detected based on the metal barium (Ba) and the nonmetal sulfur (S). Quantitative analysis by ICP-MS allowed us to infer concentration- and/or time-dependent cellular uptake and accumulation, while semi-quantitative analysis by NanoSIMS image treatment facilitated determination of the subcellular dissolution of the particles, establishing a causal correlation to toxicity.

2. Materials and methods

2.1. Cell culture and growth conditions

The toxicological investigations within the scope of this work were carried out with in normal human bronchial epithelial cells (NHBE). The cultivation and application of NHBEs were performed according to [35]. NHBEs were grown out of tumor-free specimens of human bronchus obtained from partial lung resections. Patients underwent surgery at the Hospital Martha-Maria Halle-Dörlau, Germany. Each patient had individual characteristics with respect to age, sex, occupation, smoking status, pathological diagnosis and medication. None of the parameters were exclusion criteria. The tissue for the cultures was obtained from resected specimens that were removed after tumor surgery (non-targeted tissue removal for experiments). Approval of the ethics committee of the Martin-Luther-University Halle-Wittenberg, Germany, for the use of the samples for research purposes had been obtained in advance (vote of August 16, 2017, reference no.: 2016–20).

Tissue pieces were washed several times with cold PBS after removal and subsequently transported in cold Leibovitz L-15 medium. Tissue was separated from unwanted tissue mechanically, using scissors, forceps, and scalpel under sterile conditions and cleaned. Tissue pieces from the bronchus were then cut into approximately pieces of 10 mm³ and washed three times with PBS containing 1 % penicillin/streptomycin. The pieces were then placed on 60 mm culture dishes. Subsequently, serum-free airway epithelial cell growth (AECG) medium (PromoCell, Heidelberg, Germany) with supplement (0.4 % bovine pituitary extract; 0.5 ng mL⁻¹ EGF; 5 µg mL⁻¹ insulin; 0.5 µg mL⁻¹ hydrocortisone; 0.5 µg mL⁻¹ epinephrine; 6.7 ng mL⁻¹ triiodothyronine; 10 µg mL⁻¹ transferrin; 0.1 ng mL⁻¹ retinoic acid) was added. The medium was changed three times a week. After two to three weeks, the cells grew out of the tissue pieces and formed a monolayer with a confluence of about 80–90 %. These cells are referred to as the first generation. By transferring the tissue pieces to new culture dishes, further generations could be obtained. The sub-confluent cell cultures can be detached and passaged enzymatically using trypsin, as contained in the detach kit

from PromoCell (Heidelberg, Germany). First, the supernatant medium was aspirated and cells were washed with warm HBSS. Cells were detached by adding 100 μL of trypsin/EDTA- solution per 13 cm^2 of culture area and incubating for 5 min at 37 °C. After addition of 100 μL trypsin neutralization solution (TNS) per cm^2 to stop trypsinization the cell suspension was transferred to a 15 mL centrifugation tube. Cells were centrifuged at 1000 rpm for 5 min and pelleted. The cell pellet was resuspended in fresh AECG medium and cell number was determined using a Fuchs-Rosenthal chamber. To perform the experiments, cells were seeded at appropriate cell numbers and used at 40–50 % confluency for the 72 h experiments or at 60–70 % for the 24 h experiments.

2.2. Barium sulfate nanoparticles and suspension preparation

BaSO₄ nanoparticles were obtained from Huntsman/Venator, Duisburg, Germany. According to the manufacturer, the particles are uncoated and have a primary particle size of 40 nm.

Different preparation methods for BaSO₄-NP suspensions (24 h stirring, treatment in an ultrasonic bath or using an ultrasonic probe) were tested and compared. Based on microscopic images and particle size measurement by dynamic light scattering preparation of the NP suspensions with an ultrasonic probe was established as standard operating procedure. Stock solutions were subjected to ultrasonic probe treatment in sterile glass test tubes for three minutes. A SONOPLUS from Bandelin (HD3100) with sonication cup (BB 2 G) was used, which applied an energy of about 5 kJ to the suspension. Subsequently, the appropriate dilutions were prepared and also treated with ultrasound. During treatment, solutions were cooled using ice water. Suspensions were prepared in AECG medium. All stock solutions had a concentration of 10 g L⁻¹. Nanoparticle suspensions with concentrations of 10 and 100 mg BaSO₄ L⁻¹ were used for cell exposure and further experiments.

The characterization of the suspensions with respect of nanoparticle diameter and Zeta potential was carried out using dynamic light scattering on a Zetasizer (Nano Series, Nano-Sizer/Nano-ZS from Malvern). The stock solutions were diluted accordingly for the measurement so that the lens aperture of the instrument was optimal. The measurements were performed in triplicate at a measurement angle of 173° (backscatter). The measurement time was determined automatically. The method was created with the following data: Refractive index of barium sulfate is 1.64; absorbance is 0.1; measurement temperature is 25 °C with an adjustment time of 120 s; viscosity of the solvent is 0.89 mPa·s and refractive index is 1.33. Measurements were made in a DTS0012 cuvette.

2.3. Cytotoxicity assays

At the beginning of the toxicological investigations of the barium sulfate nanoparticles and the surfactants used, their effects on the viability of the cells were determined. Cytotoxicity-tests were the starting point for further investigations to determine the sub-toxic concentration range of the particles. Three different test systems were used.

2.3.1. Resazurin assay

The resazurin test is a rapid and sensitive viability test that uses the nontoxic reagent resazurin. The resazurin assay was performed in a 24-well plate. After treatment of the cells with the nanoparticles for 24 or 72 h, the medium supernatant was removed and the cells were washed three times with 37 °C PBS. Washing was followed by incubation with the 10 % resazurin solution at 37 °C for 30 or 60 min. Fluorescence was measured after both 30 minutes and 60 minutes in the plate reader at an excitation wavelength of 530 nm and an emission wavelength of 590 nm.

2.3.2. MTT assay

The MTT assay was used to determine the cytotoxicity of the

surfactant required for suspension preparation and was performed analogously to the resazurin assay protocol. After washing the cells with warm PBS, the cells were incubated with the MTT-use solution at 37 °C for 30 min. After incubation, the cells were washed again and incubated with a mixture of formic acid and isopropanol (5:95). The measurement was made in a glass cuvette in the photometer against a blank.

2.3.3. Lactate dehydrogenase assay

The lactate dehydrogenase assay is a viability test that determines membrane integrity. For the LDH assay, 25 μL of cell supernatant from controls or treated cells, respectively, were transferred to a well of a 96-well plate. Then, 125 μL of a 0.4 mM NADH solution and 125 μL of a 2 mM sodium pyruvate solution were sequentially added to every well, without delay and free of air bubbles. The plate was transferred to a plate reader and measurement of absorption (340 nm) was performed over twelve cycles (one cycle corresponds to 90 s).

2.4. Biochemistry assays for cell culture characterization

2.4.1. Determination of cellular glutathione-content

Cellular glutathione was determined as total glutathione. After reduction of the oxidized GSH (GSSG) with 1,4- dithiothreitol, specific derivatization of the GSH with monobromobimane, modified according to Newton et al., was conducted [36] and GSH was quantified by HPLC with fluorescence detection. For the experiments cells were cultured in 6 cm dishes. After incubation of the cells with particles for 24 or 72 h, they were carefully washed with warm PBS and harvested by trypsinization. The cell pellet obtained by centrifugation was frozen away at -80 °C until further processing. After thawing, the pellet was lysed in 0.1 N HCl and sonicated for 3 min. Subsequently, the cell suspension was centrifuged at 13,000 rpm for 20 min at 4 °C. The supernatant was used to determine GSH content and protein content by bicinchoninic acid assay. For determination of GSH content, 120 μL of the supernatant were mixed with 180 μL CHES and 30 μL DTT and vortexed briefly. After incubation in the refrigerator (4 °C) for one hour, 10 μL of monobromobimane (mBrB) were added to each sample. After mixing the samples thoroughly, they were incubated for 15 min at room temperature (protected from light). The reaction was stopped with 250 μL of 5 % acetic acid. Before measurement, the samples were vortexed and centrifuged briefly. Chromatographic conditions were as follows: stationary phase was an RP-18 column (Chromolith RP-18 100-4.6 mm) with an RP-C18 end capped pre-column, also from Chromolith. The mobile phase consisted of two different eluents (phase A: 2 % methanol / 98 % H₂O / 0.25 % acetic acid (100 %) (pH 4.3) and phase B: 90 % methanol/ 10 % H₂O/ 0.25 % acetic acid (100 %) (pH 3.9)). The flow rate was 3 mL min⁻¹. For each sample, a volume of 30 μL was injected into the HPLC. Detection was performed by fluorescence detector with wavelengths λ_{exc} 380 nm and λ_{em} 480 nm.

For comparability of glutathione levels, protein content of the samples was determined and used as a reference ($\mu\text{g}/\text{mg}$ protein). Determination was made by bicinchoninic acid test. For this purpose, 10 μL of the cell supernatant of cells lysed in 0.1 N HCl, were incubated with 200 μL of a copper (II) solution and bicinchoninic acid (BCA) for 30 min at 37 °C, followed by photometric measurement of absorbance at 562 nm. A dilution series of serum albumin (BSA) in the concentration range of 0.1–1 mg mL⁻¹ BSA served as calibration.

2.4.2. Detection of induced apoptosis

Induction of apoptosis was measured by flow cytometry in a MUSE cell analyzer. Cells were seeded onto 6 cm dishes and incubated with BaSO₄-NPs for 24 or 72 h until they reached the appropriate confluence. Then the medium was removed and cells were washed twice with warm HBSS. Trypsinization was performed for exactly 5 min at 37 °C. The reaction was stopped with TNS and the detached cells were transferred to a centrifugation tube. Cells were centrifuged for 5 min at 1000 rpm at 20 °C and the resulting cell pellet was resuspended in warm PBS. 50 μL

of the cell suspension were transferred to an Eppendorf tube, that already contained 5 μL of FBS. Subsequently, 50 μL of the reagent solution were added, samples were mixed well and incubated for 20 min in the dark. The measurement was performed with the appropriate instrument program and separate adjustment or optimization of the parameters. Untreated samples resuspended in AECG medium after harvesting and then incubated at 55 °C for 30 min served as positive controls.

2.5. Cellular uptake of BaSO₄-NPs quantified by ICP-MS

Uptake of BaSO₄-NPs into the cells was quantified by inductively coupled plasma mass spectrometry (ICP-MS). Cells were seeded onto 6 cm dishes and incubated with the particles for 24 h and 72 h, respectively. After repeated and careful washing of the cells with warm PBS, cells were harvested using the Detach kit. The cell pellet was resuspended in PBS and the cell number per milliliter was determined. The resulting pellet was suspended in concentrated 67 % (w/v) HNO₃ trace metal grade (BDH Prolabo®, VWR, Darmstadt, Germany) and mineralized at 70 °C for 2 h. Samples were diluted to a final concentration of 2 % (w/v) nitric acid. Indium was added as an internal standard at a final concentration of 10 ppb. Elemental analysis was performed via ICP-MS using the ESI-sampler SC-2 (Elemental Scientific Inc., Omaha, NE, USA) and an X-Series II ICP-MS instrument (Thermo Fisher Scientific, Bremen, Germany) operating with a collision/reaction cell and flow rates of 5 mL/min of He/H₂ 93 % / 7 %, with an Ar carrier flow rate of 0.76 L min⁻¹ and an Ar make-up flow rate of 15 L min⁻¹. An external calibration curve was recorded with ICP-multi element standard solution XVI (Merck, Darmstadt, Germany) in 2 % nitric acid. Each sample was introduced via a peristaltic pump and analyzed for its metal content. For blank measurement and quality / quantity thresholds, calculations were performed based on DIN32645 (standard procedure describing decision limit, detection limit, and determination limit in chemical analysis under repeatability conditions terms, methods, evaluation; ICS Code 71.040.01). Results were transformed from barium concentrations ($\mu\text{g L}^{-1}$) to the amount of barium per 10⁶ cells.

The release of barium ions from the suspended nanoparticles into the cell culture medium was quantified using ICP-MS, too. Suspensions with concentrations of 10 and 100 mg BaSO₄ L⁻¹ in AECG medium were left at 37 °C for 72 h under the same conditions as in the cell incubation experiments. Subsequently, 5 mL of the NP suspension were transferred by pipette into a Sartorius centrifugation tube with filter unit (3 kDa). Centrifugation was carried out for 60 min at 4000 rpm and 20 °C. The barium concentration was determined in the filtrate.

2.6. Sample preparation for NanoSIMS analyses and TEM observations

After cultivation and exposure to BaSO₄-NP, cells were fixed directly with 3 % glutaraldehyde (Sigma, Taufkirchen, Germany) in 0.10 M sodium cacodylate buffer (SCB) for 3 h, centrifuged at 5000 rpm for 5 min and taken up in 4 % agar/SCB, followed by one wash-step with SCB-buffer overnight at 4 °C and three wash-steps with the same buffer for 5 min. For TEM analysis the samples were postfixed with 1 % osmium (VIII) tetroxide in SCB for 1 h. After washing with H₂O, samples were dehydrated in a graded series of ethanol (30 min with 10 %, 30 %, 50 %, 70 %, 90 %, and two times 100 % ethanol). Thereafter, samples were infiltrated with Spurr's epoxy resin and polymerized at 70 °C. Ultrathin sections of 80 and 300 nm were cut with an Ultracut R ultramicrotome (Leica, Wetzlar, Germany). The 80 nm ultrathin sections were placed on formvar coated copper grids for TEM and the 300 nm sections were placed on silicon wafers for NanoSIMS analysis. TEM observations were done with an EM900 transmission electron microscope (Carl Zeiss Microscopy, Oberkochen, Germany) operating at 80 kV. Images were recorded using a Variospeed SSCCD camera SM-1k-120 (TRS, Moorweis, Germany). TEM images were processed using the open-source software Fiji (<https://fiji.sc>) for linear contrast and brightness

adjustment and measurement of the NP size.

2.7. NanoSIMS analysis

The elemental distribution of non-metals, micronutrients, and trace metals was analyzed on the 300 nm sections with a NanoSIMS 50 L (Cameca, Gennevilliers, France), equipped with seven parallel electron multiplier detectors. A Cs⁺ ion source was used for the mapping of carbon (¹²C₂), nitrogen (¹²C¹⁴N⁻), sulfur (³²S⁻), and phosphorus (³¹P⁻) in previously selected cells (via the build-in CCD camera), with a current of 0.15 pA. Areas of 50 $\mu\text{m} \times 50 \mu\text{m}$ were pre-sputtered (10 min at 100 pA, for cesium implantation in order to increase the secondary ion yield). Subsequently, a region of 40 $\mu\text{m} \times 40 \mu\text{m}$ was analyzed with 512 \times 512 pixels and a dwell time of 10 ms per pixel. The cluster ion ¹²C¹⁴N⁻ was detected to maximize the signal measured for ¹⁴N, and the mapping of ¹²C, originating from the resin, was used to control homogeneous sputtering of the area. A Hyperion™ RF plasma O⁻ ion source was used to map carbon (¹²C⁺), sodium (²³Na⁺), and two barium isotopes (¹³⁵Ba⁺ and ¹³⁸Ba⁺) with a current between 0.20 pA and 1.7 pA. Areas of 50 $\mu\text{m} \times 50 \mu\text{m}$ were pre-sputtered (2 min at 200 pA) and then regions between 32 $\mu\text{m} \times 32 \mu\text{m}$ and 45 $\mu\text{m} \times 45 \mu\text{m}$ were analyzed with 512 \times 512 pixels and 10 ms dwell time. Again, the mapping of ¹²C was used to control homogeneous sputtering of the resin, while the two isotopes of barium were used to ensure the accuracy of mass calibration and the lack of interferences. Mass calibration was performed with element standards obtained from standard solutions (PlasmaCAL, SPC Science, Canada) dropped and evaporated on silicon wafers. Mass resolution was optimized to resolve possible interferences, but entrance and aperture slits were open to allow maximum transmission of ions of the trace elements, which resulted in a mass resolution of ~3000–5000. Three maps of the same area were acquired and stacked to obtain the final image. Image processing was performed using the software WinImage (Cameca). A logarithmic scale was applied to the barium images to visualize the dissolution of trace amounts of barium from the NPs into the cytoplasm of the cells (when indicated in the figure caption). Semi-quantitative estimation of barium dissolution was performed with the Fiji open-source software (<https://fiji.sc>). From the ¹³⁸Ba isotope, thresholds were defined for barium counts to select each region of interest (ROI): the highest 0.25 % of the barium counts in an image were used to select the ROI containing the nanoparticles, the next lower 0.25–2 % to select the ROI of dissolved barium around the nanoparticles and the next lower 25 % to select the ROI of dissolved barium inside the cell. The bottom 75 % were pixels with only one count, which was considered to be part of the background noise. In this way ROIs within the selected thresholds were established and the area inside (by pixel number) the total intensity and the mean intensity were determined. The background barium signal was calculated from the images of unexposed cells, and subtracted from the barium signal in each region. Then, these values were used to calculate the percentage of barium in each ROI with respect to the total barium signal in the image. Calculations were done for 3 NHBE cells of each condition (unexposed, 10 and 100 mg BaSO₄ L⁻¹ nanoparticle suspension) after 72 h and the results were averaged. Results are given in Table 2.

3. Results and discussion

3.1. Characterization of the BaSO₄-NP suspension

Microscopic observation of the BaSO₄-NP (Huntsman nanomaterials) suspensions showed that the most uniform particle distribution was achieved using an ultrasonic probe or ultrasonic bath for preparation. In contrast, stirring for 24 hours resulted in very inhomogeneous suspensions. Characterization of the suspensions using dynamic light scattering (DLS), which determines the hydrodynamic diameter of the NP in suspension, confirmed the uniform and stable size distribution of the particles when the suspension was processed using an ultrasonic probe.

Since primary cells were incubated with the particle suspension, barium sulfate (NPs) had to be suspended in the culture medium. Additionally, the surfactant Dispex AA4040 (BASF, Ludwigshafen, Germany) was added to the AECG medium to obtain a homogeneous nanoparticle suspension. A MTT assay to investigate the cytotoxicity of the surfactant revealed that 0.005 % surfactant addition to the AECG medium resulted in an approximate 10 % loss of viability in NHBECS.

Hydrodynamic diameter and Zeta potential were determined by DLS in triplicate for suspensions in AECG medium with surfactant as well as in water. As expected, the hydrodynamic diameter of around 100 nm was larger than the primary particle size of 40 nm specified by the manufacturer, due to the presence of a solvent layer of surfactant and water molecules around the particles (see Table 1). Several studies have addressed the challenges and peculiarities of nanosuspension preparation as well as the influence of the constituents of the medium on toxicity [37–39].

In addition, the release of Ba^{2+} ions from the $BaSO_4$ -NP suspension into the cell culture medium was determined by ICP-MS after 72 h in AECG medium. When using the lower concentrated suspension (10 mg $BaSO_4 L^{-1}$) 0.128 mg $Ba^{2+} L^{-1}$ (equivalent to 0.218 mg $BaSO_4 L^{-1}$) were found in the medium, while the higher concentrated (100 mg $BaSO_4 L^{-1}$) suspension released 0.273 mg $Ba^{2+} L^{-1}$ (equivalent to 0.464 mg $BaSO_4 L^{-1}$). This dose-dependent release of barium ions into the medium indicated that the solution equilibrium of barium sulfate (2.2 mg $BaSO_4 L^{-1}$) was far from being reached within 72 h.

The dissolution of nanoparticles is dependent on their size, shape [40], coating and possible agglomeration or aggregation. Moreover, incubation time, pH of the medium (pH 7.6 for AECG medium) and its components such as various inorganic salts, influence the solubility of barium sulfate. For example, Keller et al. found 2.9 mg $Ba^{2+} L^{-1}$ in phagolysosomal simulant fluid (pH 4.5) after suspension of $BaSO_4$ -NP for 28 days. Considering the relative fraction of Ba^{2+} ions released from the particles in our experiment, 2.18 % of the total barium was dissolved from the less concentrated suspension, while only 0.46 % was dissolved from the higher concentrated suspension. This effect indicates possible aggregation – and thus reduced specific surface area – of the particles in the higher concentrated suspension, leading to a reduced dissolution of barium sulfate. Although suspending particles in a medium, incubating, removing the remaining solids and analyzing the analyte in solution is a common approach to assess the solubility of nanoparticles, it must be considered that the static abiotic solubility measured in this way may differ from the dynamic dissolution processes of nanoparticles *in vivo* [41].

3.2. Cellular uptake

The cellular uptake of $BaSO_4$ -NPs in normal human bronchial epithelial cells (NHBECS) was demonstrated by barium determination by ICP-MS, showing a dose-dependent increase in barium concentration within the cells (Fig. 1). This roughly reflects the ratio of the $BaSO_4$ concentrations (Huntsman nanomaterials) of both suspensions. However, a clear dependence on the exposure time could not be observed. The uptake of $BaSO_4$ particles by other cell types has also been demonstrated. Sokolova et al. [42] studied primary phagocytosing mouse bone marrow cells and found that both dendritic cells and macrophages took up particles of sizes 40 nm, 420 nm, and 1 μm in a dose- and time-dependent manner, with macrophages having a higher particle

Table 1

Hydrodynamic diameter and Zeta potential of the barium sulfate nanoparticle (Huntsman nanomaterials) suspension.

Parameter	Value
d [nm] AECG/0.005 % Dispex	107 ± 5
d [nm] H ₂ O	93 ± 7
Zeta- Potential [mV] AECG/0.005 % Dispex	−25,4

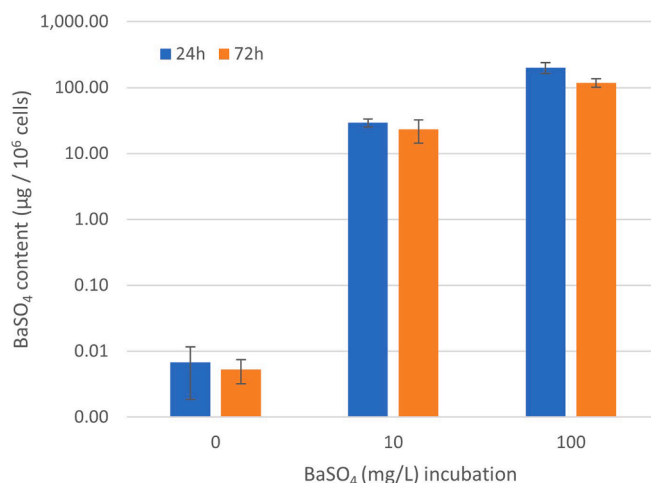


Fig. 1. Quantitative uptake of $BaSO_4$ -NP into NHBECS after incubation with $BaSO_4$ suspensions in different concentrations for 24- and 72-hour, compared to untreated controls. Concentrations determined by quantitative ICP-MS analysis of barium ($n = 3$).

concentration inside than dendritic cells. Particles were localized in phagosomes and heterophagosomes, confirming NP uptake via phagocytosis [43]. In a recent study, Lehner et al. [44] demonstrated uptake of poorly soluble NP of $BaSO_4$, CeO_2 , TiO_2 , and ZnO at the lung epithelial tissue barrier and into different cell compartments through cellular fractionation and ICP-OES analysis.

3.3. Toxic effects of $BaSO_4$ nanoparticles on NHBECS

Various toxicological endpoints were analyzed in order to gain insight into the mechanisms of the effects of $BaSO_4$ nanoparticles (Huntsman nanomaterials) on normal human bronchial epithelial cells (NHBECS) after incubation for 24 h and 72 h, respectively. A loss of viability of up to 20 % was defined as a subtoxic concentration range. Experiments to determine glutathione content and induction of apoptosis were performed within this concentration range or slightly above it (i.e., in the mildly toxic range).

3.3.1. Resazurin assay

The resazurin assay demonstrated a dose- and - at higher exposure concentrations - a time-dependent loss of viability of NHBECS when treated with nanoscale $BaSO_4$. After 24 h and 72 h exposure to 10 mg $BaSO_4$ -NP L^{-1} , NHBECS showed a decrease in viability to about 90 % but not significant without clear effect of exposure time. With increasing concentrations time dependence could additionally be observed. Incubation with a $BaSO_4$ -NP concentration of 100 mg L^{-1} resulted to a not significant decrease in viability to 87 % after 24 h, however, after 72 h of treatment, viability decreased significantly to 69 %. At the highest concentration of 1000 mg $BaSO_4$ -NP L^{-1} , the viability was still 80 % after 24 h, but dropped to only 28 % after 72 h of treatment (Fig. 2).

3.3.2. LDH assay

A significant increase in lactate dehydrogenase (LDH) activity in the medium, which would have indicated cell membrane damage, could not be measured in the LDH assay at $BaSO_4$ concentrations up to 1000 mg L^{-1} . The positive control (PK; 0.01 % TritonX-100) resulted in significant LDH activity in the assay (data not shown).

3.3.3. Glutathione content

The intracellular glutathione content of primary cells was determined by HPLC after acid lysis of the cells, reduction of GSSG and derivatization of the total amount of GSH with monobromobimane. Determination of the intracellular GSH content allows conclusions to be

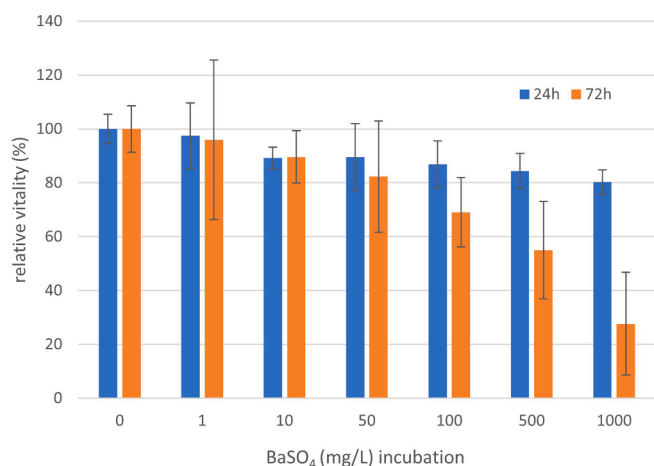


Fig. 2. Relative viability of NHBE cells in resazurin assay after incubation with BaSO₄ suspensions in different concentrations for 24 and 72 hours, compared to controls (n = 3). Relative viability is shown related to untreated controls (100 % viability).

drawn about the formation of reactive oxygen species (ROS). GSH is the most important antioxidant in human cells. Under the influence of ROS, the reduced form of GSH is oxidized to GSSG and an altered GSH/GSSG ratio can lead to increased GSH synthesis [45]. Treatment of NHBE cells with 10 and 100 mg L⁻¹ nanoscale BaSO₄ for 24 h caused no change in GSH content, nor did it show any effect on GSH content after 72 h of incubation (data not shown). Thus, no indication of ROS formation could be found in these experiments under the selected conditions.

3.3.4. Apoptosis assay

Treatment of NHBE cells with nanoscale BaSO₄ up to 1000 mg L⁻¹ for 24 h and 72 h, respectively, resulted in no induction of apoptosis (data not shown). Treatment of cells at 55 °C for 30 min induced apoptosis in

approximately 50 % or more of the cells, demonstrating that primary cells are sensitive to apoptotic stressors and that this treatment is suitable as a positive control. Thus, no evidence of BaSO₄-NPs-induced apoptosis could be found in this experiment under the chosen conditions.

3.4. TEM and NanoSIMS analysis of BaSO₄-NP uptake and localization in NHBE cells

Based on the results of the viability assay, 72-hour incubations with nanoparticle suspensions of 10 mg BaSO₄ L⁻¹ (no cytotoxic effect) and 100 mg BaSO₄ L⁻¹ (mild cytotoxic effect) were chosen for subcellular investigations of NHBE cells. Sections of resin-embedded control and exposed NHBE cells were investigated using transmission electron microscopy (TEM) and nanoscale secondary ion mass spectrometry (NanoSIMS) to examine nanoparticle uptake and subcellular localization.

3.4.1. TEM observations

TEM images (Fig. 3) allowed the identification of key cellular structures such as nucleus, nucleolus and vesicles of the NHBE cells. After 72 h of exposure to both 10 mg BaSO₄ L⁻¹ and 100 mg BaSO₄ L⁻¹ nanoparticle suspensions, numerous BaSO₄-NPs could be observed as black spots within the vesicles. Cells exposed to the suspension with the higher concentration exhibited a greater number of NPs and more pronounced aggregation.

Size measurement of individual NP in TEM images revealed an average size of 41 ± 9 nm, corroborating the manufacturer's information. Based on the cellular uptake of barium determined by ICP-MS in this study, high amounts of NPs were expected inside the NHBE cells. Although the TEM images represent ultra-thin sections of only a few single cells and thus lack statistical significance, the observations of dense areas with barium sulfate nanoparticles suggest a substantial number of NPs throughout the entire cells. These findings align with other studies, such as one involving rats instilled with 1 mg BaSO₄ L⁻¹ which also demonstrated significant internalization of BaSO₄-NPs into

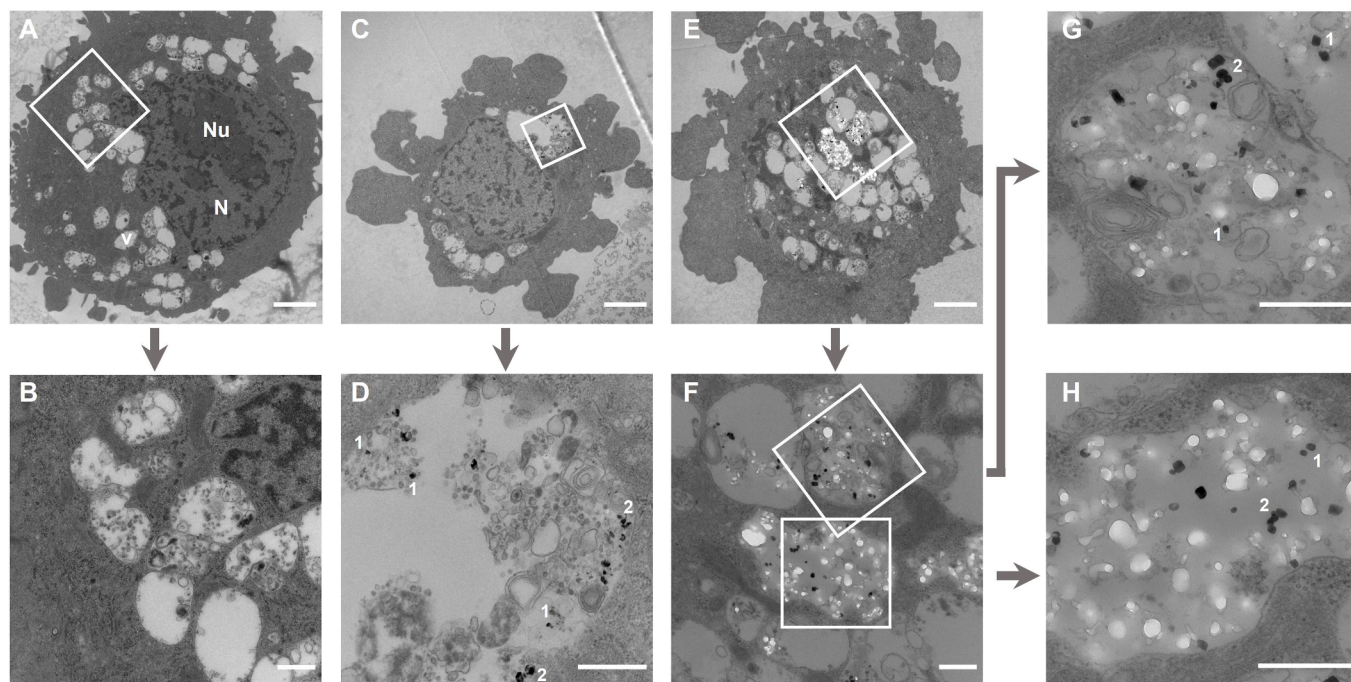


Fig. 3. TEM images of NHBE cells. (A) Control (unexposed) cell showing the nucleus (N) the nucleolus (Nu), and vesicles (v). (B) Magnification of vesicles of the control cell. (C) Cell exposed to 10 mg BaSO₄ L⁻¹ suspension and (D) magnification of vesicles with (1) single NP and (2) aggregation of NP. (E) Cell exposed to 100 mg BaSO₄ L⁻¹ suspension and (F, G, H) magnifications of vesicles with single NP (1) and aggregation of NP (2). Scale bars 2 μm (A, C, E) and 500 nm (B, D, F, G, H).

lung alveolar macrophages and type II epithelial cells observed by TEM [46].

3.4.2. NanoSIMS imaging

NanoSIMS imaging of NHBEs was performed using two different primary ion beams: Cs^+ and O^- . The Cs^+ primary ion beam was employed for mapping of non-metals (N, P, S), while the O^- primary ion beam was used for mapping of barium isotopes and other metals (Na) in a subsequent analysis of the same area.

Nitrogen maps (measured via the CN^- cluster ion) indicated predominantly protein distribution, thus revealing the cellular structure as observed in TEM, while mapping of phosphorus highlighted the nucleus and nucleolus in addition to the general cellular structure. In control cells, the sulfur maps displayed the basal sulfur distribution mainly from sulfur-containing proteins, mirroring the nitrogen images. Using the O^- primary ion source, sodium maps also revealed the cellular structure, enabling the overlay of images obtained from both primary ion beam modes.

In control NHBEs, no barium signal could be detected, besides the background noise of the detector, confirming the absence of barium in unexposed cells (Fig. 4). In exposed NHBEs (Fig. 5 and Fig. 6), BaSO_4 -NPs were detected as small spots via the sulfur signal (obtained with the Cs^+ beam) and the signal of both barium isotopes, ^{135}Ba and ^{138}Ba (obtained with the O^- beam). The distinct overlay of ^{32}S , ^{135}Ba and ^{138}Ba signals confirmed unambiguously the identity and localization of BaSO_4 -NPs within the cytosol and vesicles of NHBEs (Fig. 5 and Fig. 6). However, an uptake of the particles into the nucleus was not observed during our experiments, which is consistent with findings from other studies [42]. NanoSIMS imaging further illustrated that higher concentrations of BaSO_4 -NP suspension (100 mg L^{-1}) led to more significant aggregation of NPs within the cells (Fig. 6).

Other studies also examined the uptake of nanoparticles into the cell

using different microscopic techniques. For example, Llop et al. showed that aluminum oxide, titanium dioxide, iron oxide, zinc oxide and cerium oxide NPs were attached to the cell surface, first, and then taken up into endosomes by lung cells. However, no particles were found inside the nucleus, too [47]. Lichtenstein et al. compared the internalization of silver and iron oxide nanoparticles in human intestinal epithelial cells (Caco-2), revealing differences in uptake of particles similar in size, shape and coating depending on the core material of the NPs [48].

When transferring toxicological *in vitro* data to the whole organism, the influence of the surfactant (consisting of phospholipids and proteins) present in the lung and the movement of cells by the respiratory process are important factors influencing particle uptake of the cells. It is known from older studies that alveolar type II (ATII) cells have increased secretion of surfactant when stretched [49]. The extent to which the surfactant in turn enhances or diminishes NP uptake and possible toxic effects is subject of current research and not fully understood, yet [50].

It has been shown that aluminum oxide (Al_2O_3), silicon dioxide (SiO_2) and latex NP can interact with surfactant simulants and NP can act as links between surfactant vesicles. This 'sticker' function is particularly pronounced when surface charges differ greatly. Some inhaled nanoparticles could thus affect the interfacial and overall properties of lung surfactant and disrupt lung physiology [51].

It is a well-established fact that, surface coating of NPs can have a decisive influence on their biological effects [52]. This was also shown in a study by Romera et al. for lipid-coated carbon nanotubes (CNTs), which showed reduced liver toxicity compared to uncoated CNTs [53].

In summary, it can be stated that, besides the intrinsic material-properties, possible toxic effects of NP are also influenced by extrinsic properties depending on the surroundings. Nevertheless, the exact correlations of properties and effects, as well as the interdependences of some material properties, still remain to be established [54]. Suggested

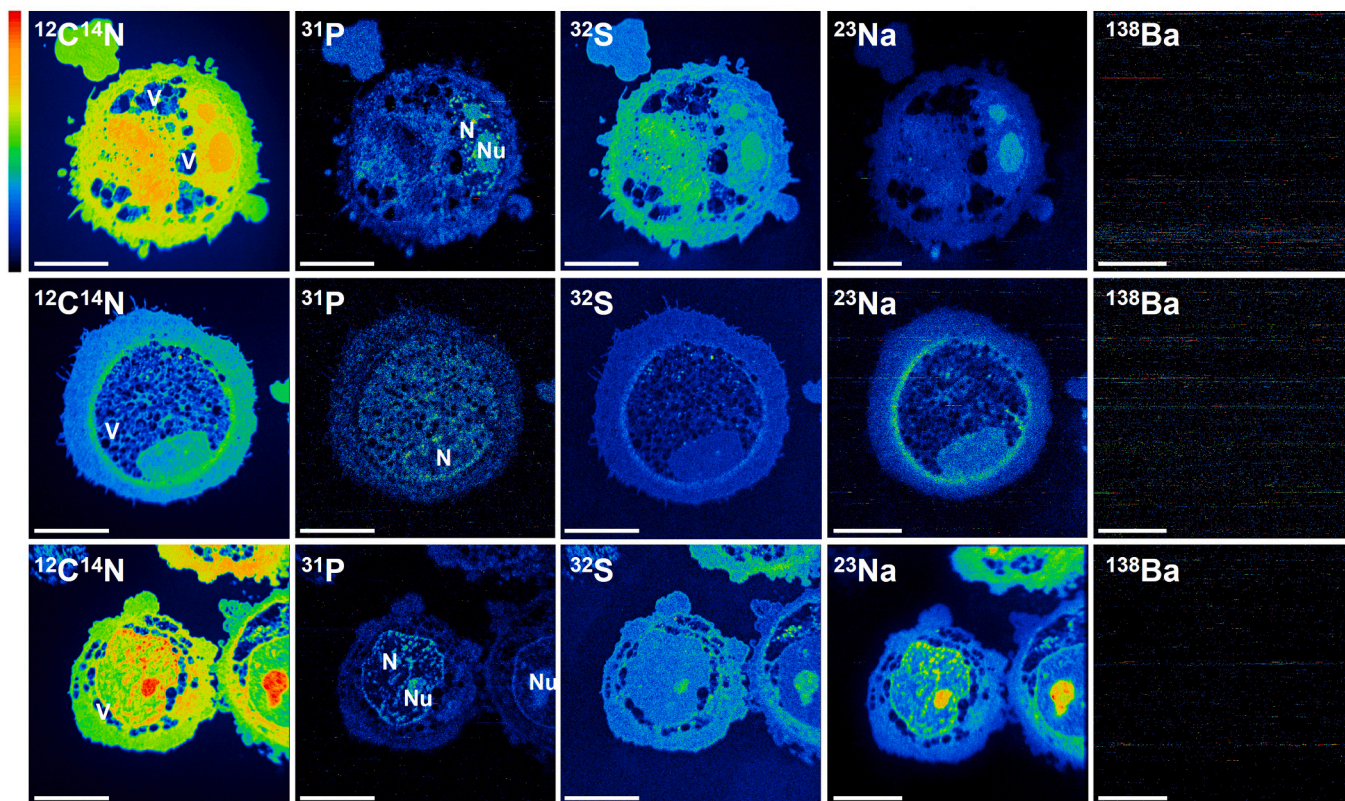


Fig. 4. NanoSIMS imaging of three control (unexposed) NHBEs using Cs^+ primary ions for $^{12}\text{C}^{14}\text{N}$, ^{31}P and ^{32}S , and O^- primary ions for ^{23}Na and ^{138}Ba mapping. Nucleus (N), nucleolus (Nu), vesicle (V). Scale bar $10 \mu\text{m}$.

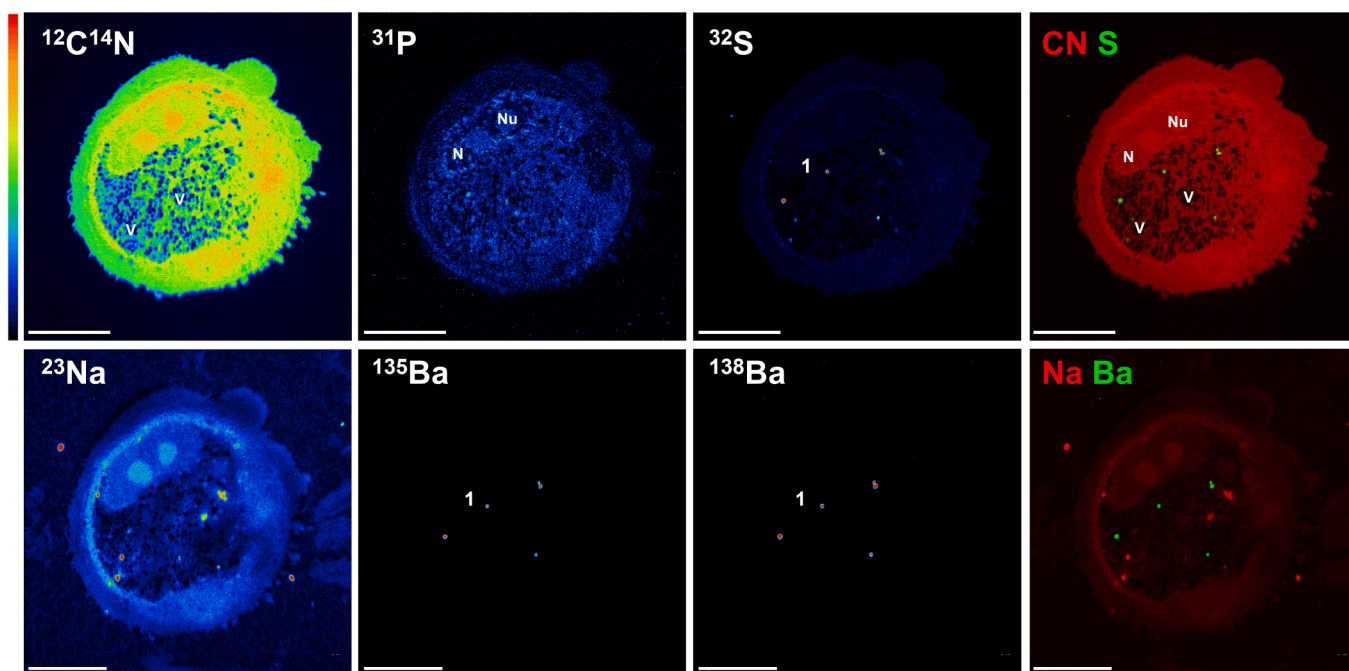


Fig. 5. NanoSIMS imaging of a NHBEC exposed to 10 mg $\text{BaSO}_4 \text{ L}^{-1}$ nanoparticles in suspension showing single NPs (1). Colocalization of sulfur and barium isotopes confirms the presence of BaSO_4 -NPs. Nucleus (N), nucleolus (Nu), vesicle (V). Scale bar 10 μm .

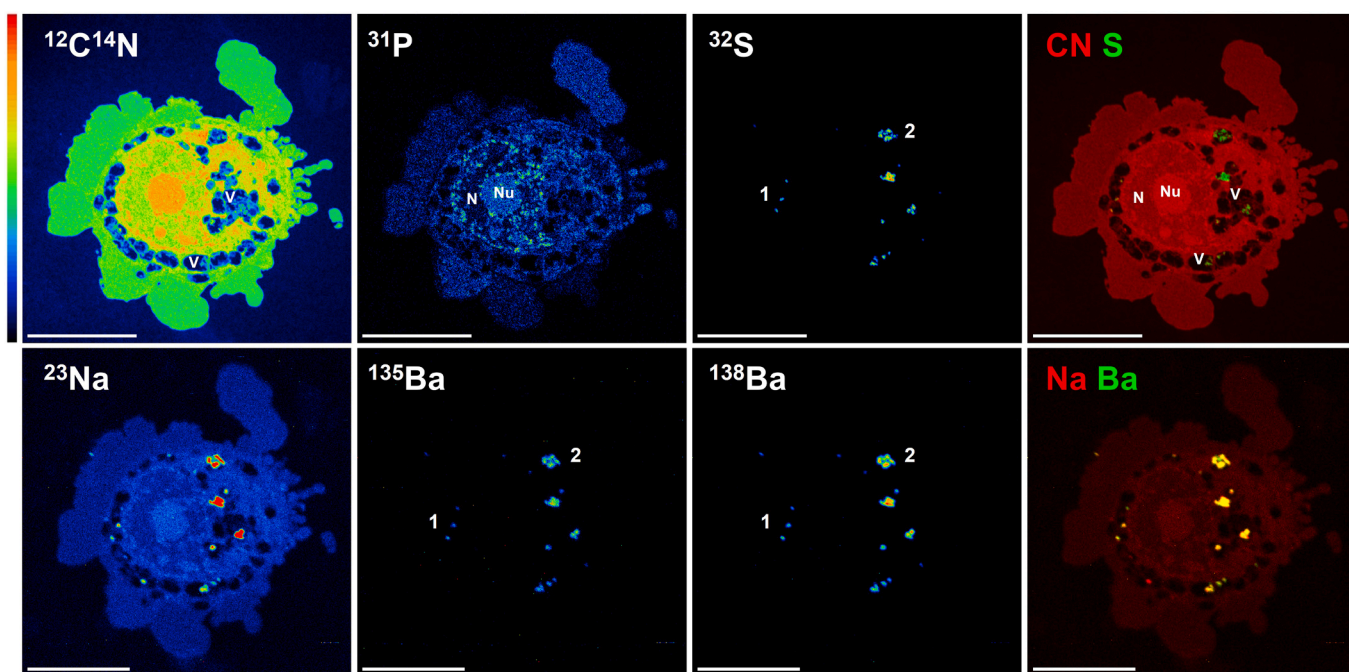


Fig. 6. NanoSIMS imaging of a NHBEC exposed to 100 mg $\text{BaSO}_4 \text{ L}^{-1}$ nanoparticles in suspension showing single NPs (1) and aggregation of NPs (2). Colocalization of sulfur and barium isotopes confirms the presence of BaSO_4 -NP. Nucleus (N), nucleolus (Nu), vesicle (V). Scale bar 10 μm .

relevant extrinsic properties comprise biological interactions, dissolution under (relevant) physiological conditions, uptake and distribution, as well as early and apical biological effects [54]. In the case of dissolving NPs sub-cellular distribution of dissolved ions or molecules should be investigated.

3.5. BaSO_4 -NPs dissolution and subcellular distribution of Ba^{2+} visualized and quantified by NanoSIMS

NanoSIMS is a high-resolution imaging technique combined with sensitive detection of trace amounts of chemical elements. As already demonstrated in this study by quantifying the release of Ba^{2+} ions from BaSO_4 -NPs to the medium via ICP-MS, these nanoparticles are poorly soluble but not insoluble. In addition to this static abiotic dissolution, dynamic particle dissolution can take place *in vivo* [46]. For example,

Konduru et al. demonstrated that in rats 28 days after intratracheally installation of BaSO₄-NPs 29 % of the barium was incorporated into the bones and 7 % into all other tissues, suggesting *in vivo* nanoparticle dissolution [14].

In our work, the dissolution of BaSO₄-NPs was detected and visualized on subcellular level by barium mapping of NHBEs using the O⁻ ion beam of the NanoSIMS. A logarithmic scale of the ion counts allows the visualization of the distribution of dissolved barium in the cell together with nanoparticles. In addition, line scans within the NanoSIMS images through areas outside and inside the cells as well as through nanoparticles demonstrate that the barium counts (15–25 cts) detected inside the cells next to the NPs are higher than the detector background noise (0–2 cts) registered outside the cells (Fig. 7 and Fig. 8). These measurements demonstrate that Ba²⁺ ions are spread throughout the whole

cell. However, this could not be observed in each cell. When nanoparticles are more aggregated, e.g., during incubation with the higher concentrated nanoparticle suspension, barium is rather detected around the aggregated particles than throughout the entire cell, as it can be seen for two cells in Fig. 8, and as demonstrated by the calculations in Table 2. In this case, higher aggregation of NPs led to less dissolution of barium sulfate as was also observed previously using ICP-MS quantification.

Secondary ion mass spectrometry (SIMS) is not considered a quantitative imaging technique due to the high matrix dependency of the ionization process. However, using the same matrix within resin-embedded cells allows for a semi-quantitative comparison of the measured counts. For the calculation of the barium distribution in the different areas within an ultrathin section of an NHBE cell, three areas

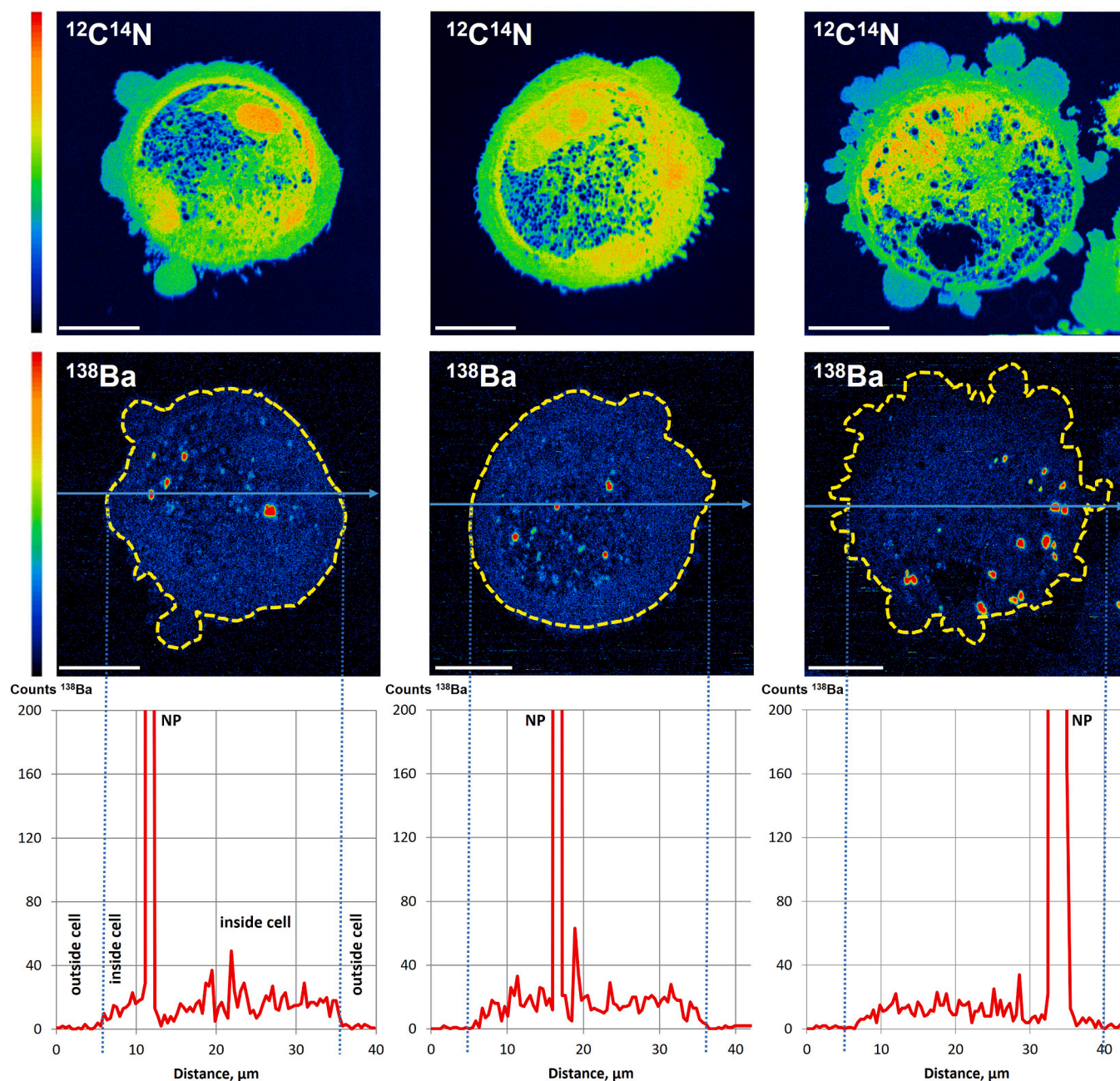


Fig. 7. NanoSIMS imaging of three NHBEs exposed to 10 mg BaSO₄ L⁻¹ nanoparticle suspension. ¹²C¹⁴N mapping shows the cell morphology. ¹³⁸Ba mapping is displayed in logarithmic scale (0–200 counts) and shows NP as well as dissolved barium in the cells. Dashed lines indicate the cell shapes. Line scans through the entire cells additionally confirm NPs and dissolved Ba. Scale bar 10 μm.

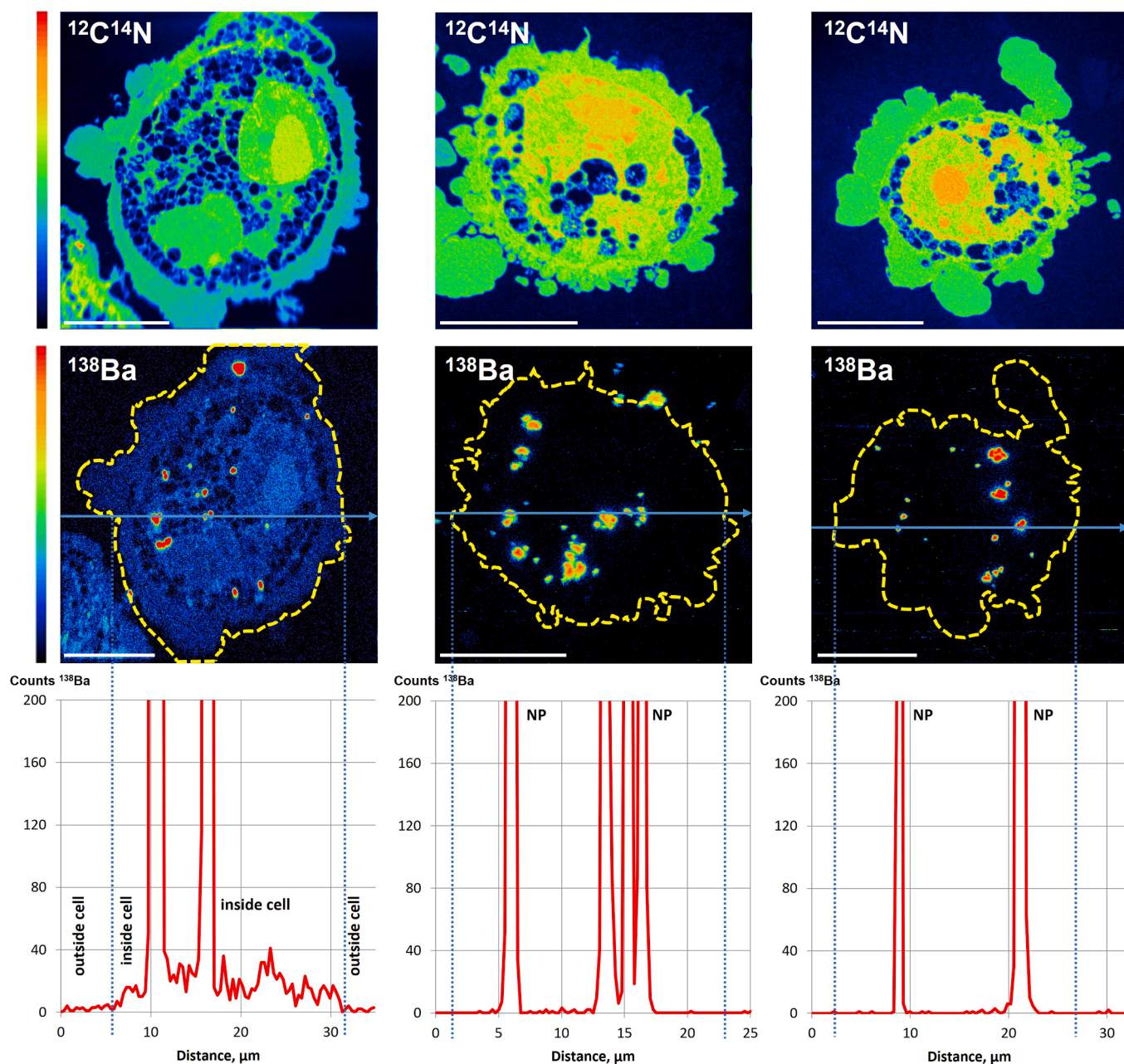


Fig. 8. NanoSIMS imaging of three NHBE cells exposed to $100 \text{ mg BaSO}_4 \text{ L}^{-1}$ nanoparticle suspension. $^{12}\text{C}^{14}\text{N}$ mapping shows the cell morphology. ^{138}Ba mapping is displayed in logarithmic scale (0–200 counts) and shows NPs as well as dissolved barium in one cell. Dashed lines indicate the cell shapes. Line scans through the entire cells additionally confirm NPs and dissolved Ba. Scale bar $10 \mu\text{m}$.

(ROIs) were distinguished: (1) the nanoparticle itself, (2) the area with higher barium concentration surrounding the particles resulting from their dissolution, thus indicating the partial dissolution of the respective particles, and (3) the low concentration barium distribution throughout the NHBE cells originating from the partial dissolution of the visible particles, but also from particles in other planes (not visible in the analyzed ultrathin section but present in the cell), and potentially from particles that have already fully dissolved. After image processing of the NanoSIMS analysis of NHBE cells sections, the results showed, as a rough estimation, that in these sections between 45 % (for the exposure to $10 \text{ mg BaSO}_4 \text{ L}^{-1}$ nanoparticle suspension) and 57 % (for the exposure to $100 \text{ mg BaSO}_4 \text{ L}^{-1}$ nanoparticle suspension) of the barium were still present in NPs, while 21 and 36 %, respectively, of the dissolved barium were located around the NPs and between 34 % and 8 % were spread over the entire cell (Table 2). This suggests that BaSO_4 -NPs dissolved to

Table 2

Percentage of the barium content, calculated from the number of ^{138}Ba counts that is present in each distinguishable part of the NHBE cells after 72 h, related to the total barium content, after removing the background signal obtained from unexposed cells. Results given as mean \pm SD with $n = 3$.

	Ba content (%)		
	Particles	Dissolution	Cell
$10 \text{ mg BaSO}_4 \text{ L}^{-1}$	45 ± 8	21 ± 16	34 ± 13
$100 \text{ mg BaSO}_4 \text{ L}^{-1}$	57 ± 22	36 ± 25	8 ± 9

a significant extent in NHBE cells within 72 h in both dose groups. However, the aggregation of nanoparticles at the higher exposure concentration reduced the dissolution of NPs and substantially reduced the amount of barium that was spread throughout the whole cell, as

previously mentioned.

Using NanoSIMS imaging, we demonstrated the uptake of BaSO₄-NPs by NHBEs for the first time, as well as a partial dissolution of these nanoparticles. Although the NPs remained in the cytosol and vesicles, the dissolved Ba²⁺ ions spread throughout the cells and penetrated into the nuclei. Cytotoxicity of BaSO₄-NPs, as demonstrated in this study by the loss of viability with increasing BaSO₄-NP concentrations (Fig. 2), and also by others after exposure of A549 cells to aerosols of BaSO₄-NPs [55] could be related to the partial dissolution of the NPs within 72 h of exposure and the presence of Ba²⁺ ions in all parts of the cells, even though BaSO₄-NPs are considered poorly soluble particles with low toxicity [5].

4. Conclusions

Our study primarily focused on the investigation of uptake and dissolution of nano-particles in cells and possible uptake of nano-particles into the nucleus. In order to gain insight into such processes occurring relatively short after exposure, experiments were conducted with short exposure times of 24 and 72 h, respectively. The cellular uptake of BaSO₄-NPs by NHBEs quantified by ICP-MS shows a dose-dependent increase in the number of particles taken up. Also, a high number of nanoscale particles were observed in the cytosol and vesicles by TEM, which was unambiguously confirmed by element-specific NanoSIMS mapping. Uptake of particles into the nucleus could not be observed in this work. However, it was found that the NPs partially dissolved and the barium spread throughout the entire cell. BaSO₄-NPs caused a dose- and time-dependent loss of viability in human lung cells. However, they did not alter the activity of lactate dehydrogenase and the associated membrane integrity. Moreover, no apoptosis was induced in NHBE. The mechanism underlying the loss of viability caused by BaSO₄-NP in our study does not seem to be associated with oxidative stress based on the measurements of the effects on the intracellular glutathione content. The extent to which released barium ions determine the toxic effect *in vitro* should be investigated in future studies through a direct comparison with a soluble barium compound. This mechanism seems to be of particular importance, also considering the results from *in vivo* experiments and the short half-life of BaSO₄ observed in those studies. Moreover, future studies should include longer exposure times as *in vivo* studies showed distribution of Ba ions in the body of experimental animals 28 days after intra-tracheal instillation.

Funding sources and acknowledgments

The work was supported by the project ANR-11-EQPX-0027 MARSS of the Agence Nationale de la Recherche, France, by the project Nano-Emission 03X3578 of the Bundesministerium für Bildung und Forschung, Germany, and by the project 35098WK of the bilateral (German-French) DAAD - Campus France program PHC PROCOPE. We also acknowledge to the DFG for providing the ICP-MS by DFG grant INST 271/266-1 to the Martin-Luther-University Halle-Wittenberg as well as Dietrich H. Nies and Heidi Foth for laboratory space provision.

Research data

Research data underlying this article are available upon request.

CRedit authorship contribution statement

Schaumlöffel Dirk: Writing – review & editing, Writing – original draft, Visualization, Funding acquisition, Data curation. **Glahn Felix:** Writing – review & editing, Supervision. **Herzberg Martin:** Writing – review & editing, Writing – original draft, Visualization, Formal analysis, Data curation. **Thomas Sarah:** Investigation, Formal analysis, Data curation. **Subirana Maria Angels:** Writing – review & editing, Writing – original draft, Visualization, Formal analysis, Data curation. **Dobritzsch**

Dirk: Writing – review & editing. **Hause Gerd:** Writing – review & editing, Formal analysis.

Declaration of Competing Interest

The authors declare that they have no known competing financial interests or personal relationships that could have appeared to influence the work reported in this paper.

References

- [1] W.J. Stark, P.R. Stoessel, W. Wohlleben, A. Hafner, Industrial applications of nanoparticles, *Chem. Soc. Rev.* 44 (16) (2015) 5793–5805.
- [2] S. Anu Mary Ealia, M.P. Saravanakumar, A review on the classification, characterisation, synthesis of nanoparticles and their application, *IOP Conference Series: Materials Science and Engineering* 263 (3) (2017) 032019.
- [3] H.M. Kipen, D.L. Laskin, Smaller is not always better: nanotechnology yields nanotoxicology, *Am. J. Physiol. Lung Cell Mol. Physiol.* 289 (5) (2005) L696–L697.
- [4] X. He, H. Zhang, Y. Ma, W. Bai, Z. Zhang, K. Lu, Y. Ding, Y. Zhao, Z. Chai, Lung deposition and extrapulmonary translocation of nano-ceria after intratracheal instillation, *Nanotechnology* 21 (28) (2010) 285103.
- [5] D. Schwotzer, H. Ernst, D. Schaudien, H. Kock, G. Pohlmann, C. Dasenbrock, O. Creutzenberg, Effects from a 90-day inhalation toxicity study with cerium oxide and barium sulfate nanoparticles in rats, *Part. Fibre Toxicol.* 14 (1) (2017) 23.
- [6] R.T. Cullen, C.L. Tran, D. Buchanan, J.M.C. Davis, A. Searl, A.D. Jones, K. Donaldson, Inhalation of poorly soluble particles. I. Differences in inflammatory response and clearance during exposure, *Inhal. Toxicol.* 12 (12) (2000) 1089–1111.
- [7] J. Wu, Y.J. Zhu, Acid/alkali-proof fire-resistant inorganic paper comprising fibers assembled from barium sulfate nanorods, *Eur. J. Inorg. Chem.* 2021 (5) (2020) 492–499.
- [8] K. Wang, J.S. Wu, H.M. Zeng, Microstructure and fracture behavior of polypropylene/barium sulfate composites, *J. Appl. Polym. Sci.* 99 (3) (2006) 1207–1213.
- [9] C.H.J. Basten, J.C. Kois, The use of barium sulfate for implant templates, *J. Prosthet. Dent.* 76 (4) (1996) 451–454.
- [10] W. Tanomkiat, W. Galassi, Barium sulfate as contrast medium for evaluation of postoperative anastomotic leaks, *Acta Radio.* 41 (5) (2000) 482–485.
- [11] A. Ricker, P. Liu-Snyder, T.J. Webster, The influence of nano MgO and BaSO₄ particle size additives on properties of PMMA bone cement, *Int J. Nanomed.* 3(1) (2008) 125–132.
- [12] G.E. Aninwene, D. Stout, Z.F. Yang, T.J. Webster, Nano-BaSO₄: a novel antimicrobial additive to pelleted, *Int J. Nanomed.* 8 (2013) 1197–1205.
- [13] H.S. Choi, Y. Ashitake, J.H. Lee, S.H. Kim, A. Matsui, N. Insin, M.G. Bawendi, M. Semmler-Behnke, J.V. Frangioni, A. Tsuda, Rapid translocation of nanoparticles from the lung airspaces to the body, *Nat. Biotechnol.* 28 (12) (2010) 1300–1303.
- [14] N. Konduru, J. Keller, L. Ma-Hock, S. Groters, R. Landsiedel, T.C. Donaghey, J. D. Brain, W. Wohlleben, R.M. Molina, Biokinetics and effects of barium sulfate nanoparticles, *Part. Fibre Toxicol.* 11 (1) (2014) 55.
- [15] R.M. Molina, N.V. Konduru, R.J. Jimenez, G. Pyrgiotakis, P. Demokritou, W. Wohlleben, J.D. Brain, Bioavailability, distribution and clearance of tracheally instilled, gavage or injected cerium dioxide nanoparticles and ionic cerium, *Environ. Sci.: Nano* 1 (6) (2014) 561–573.
- [16] J. Seiffert, F. Hussain, C. Wiegman, F. Li, L. Bey, W. Baker, A. Porter, M.P. Ryan, Y. Chang, A. Gow, J. Zhang, J. Zhu, T.D. Tetley, K.F. Chung, Pulmonary toxicity of instilled silver nanoparticles: influence of size, coating and rat strain, *PLoS One* 10 (3) (2015) e0119726.
- [17] W.G. Kreyling, W. Moller, U. Holzwarth, S. Hirn, A. Wenk, C. Schleh, M. Schaffler, N. Haberl, N. Gibson, J.C. Schittny, Age-dependent rat lung deposition patterns of inhaled 20 nm diameter gold nanoparticles and their quantitative biokinetics in adult rats, *ACS nano* 12 (8) (2018) 7771–7790.
- [18] D. Schaumlöffel, R. Hutchinson, J. Malherbe, P.L. Coustumer, E. Gontier, M. P. Isaure, Novel Methods for Bioimaging Including LA-ICP-MS, NanoSIMS, TEM / X-EDS, and SXRF, in: B. Michalke (Ed.), *Metallomics*, Wiley, 2016, pp. 83–116.
- [19] J. Malherbe, F. Penen, M.P. Isaure, J. Frank, G. Hause, D. Dobritzsch, E. Gontier, F. Horreard, F. Hillion, D. Schaumlöffel, A new radio frequency plasma oxygen primary ion source on nano secondary ion mass spectrometry for improved lateral resolution and detection of electropositive elements at single cell level, *Anal. Chem.* 88 (14) (2016) 7130–7136.
- [20] M. Senoner, W.E.S. Unger, SIMS imaging of the nanoworld: applications in science and technology, *J. Anal. At. Spectrom.* 27 (7) (2012) 1050–1068.
- [21] M.A. Subirana, D. Schaumlöffel, Imaging of Nanopollutants at Sub-cellular Resolution by Nanoscale Secondary Ion Mass Spectrometry, in: J. Szpunar, J. Jiménez-Lamana (Eds.), *Environmental Nanopollutants*, The Royal Society of Chemistry, 2022, pp. 389–413.
- [22] J.N. Audinot, A. Georgantzopoulou, J.P. Piret, A.C. Gutleb, D. Dowsett, H. N. Migeon, L. Hoffmann, Identification and localization of nanoparticles in tissues by mass spectrometry, *Surf. Interface Anal.* 45 (1) (2013) 230–233.
- [23] R. Sekine, K.L. Moore, M. Matzke, P. Vallotton, H. Jiang, G.M. Hughes, J.K. Kirby, E. Donner, C.R.M. Grovenor, C. Svendsen, E. Lombi, Complementary imaging of silver nanoparticle interactions with green algae: dark-field microscopy, electron microscopy, and nanoscale secondary ion mass spectrometry, *ACS nano* 11 (11) (2017) 10894–10902.

- [24] S. Wang, J. Lv, J. Ma, S. Zhang, Cellular internalization and intracellular biotransformation of silver nanoparticles in *Chlamydomonas reinhardtii*, *Nanotoxicology* 10 (8) (2016) 1129–1135.
- [25] L. Zhang, H. Jiang, W.-X. Wang, Subcellular Imaging of Localization and Transformation of Silver Nanoparticles in the Oyster Larvae, *Environ. Sci. Technol.* 54 (18) (2020) 11434–11442.
- [26] Z. Shao, P. Guagliardo, H. Jiang, W.X. Wang, Intra- and intercellular silver nanoparticle translocation and transformation in oyster gill filaments: coupling nanoscale secondary ion mass spectrometry and dual stable isotope tracing study, *Environ. Sci. Technol.* 55 (1) (2021) 433–446.
- [27] K. Mehennaoui, S. Cambier, T. Serchi, J. Ziebel, E. Lentzen, N. Valle, F. Gueroled, J. S. Thomann, L. Giamberini, A.C. Gutleb, Do the pristine physico-chemical properties of silver and gold nanoparticles influence uptake and molecular effects on *Gammarus fossarum* (Crustacea Amphipoda)? *Sci. Total Environ.* 643 (2018) 1200–1215.
- [28] A. Georgantzopoulou, Y.L. Balachandran, P. Rosenkranz, M. Dusinska, A. Lankoff, M. Wojewodzka, M. Kruszewski, C. Guignard, J.N. Audinot, S. Girija, L. Hoffmann, A.C. Gutleb, Ag nanoparticles: size- and surface-dependent effects on model aquatic organisms and uptake evaluation with NanoSIMS, *Nanotoxicology* 7 (7) (2013) 1168–1178.
- [29] A. Georgantzopoulou, T. Serchi, S. Cambier, C.C. Leclercq, J. Renaut, J. Shao, M. Kruszewski, E. Lentzen, P. Grysan, S. Eswara, J.N. Audinot, S. Contal, J. Ziebel, C. Guignard, L. Hoffmann, A.J. Murk, A.C. Gutleb, Effects of silver nanoparticles and ions on a co-culture model for the gastrointestinal epithelium, *Part. Fibre Toxicol.* 13 (1) (2016) 9.
- [30] S. Bettini, E. Boutet-Robinet, C. Cartier, C. Comera, E. Gaultier, J. Dupuy, N. Naud, S. Tache, P. Grysan, S. Reguer, N. Thieriet, M. Refregiers, D. Thiaudiere, J. P. Cravedi, M. Carriere, J.N. Audinot, F.H. Pierre, L. Guzylack-Piriou, E. Houdeau, Food-grade TiO₂ impairs intestinal and systemic immune homeostasis, initiates preneoplastic lesions and promotes aberrant crypt development in the rat colon, *Sci. Rep.* 7 (1) (2017) 40373.
- [31] V.R. Lopes, V. Loitto, J.N. Audinot, N. Bayat, A.C. Gutleb, S. Cristobal, Dose-dependent autophagic effect of titanium dioxide nanoparticles in human HaCaT cells at non-cytotoxic levels, *J. Nanobiotechnology* 14 (1) (2016) 22.
- [32] J.P. Piret, D. Jacques, J.N. Audinot, J. Mejia, E. Boilan, F. Noel, M. Fransolet, C. Demazy, S. Lucas, C. Saout, O. Toussaint, Copper(II) oxide nanoparticles penetrate into HepG2 cells, exert cytotoxicity via oxidative stress and induce pro-inflammatory response, *Nanoscale* 4 (22) (2012) 7168–7184.
- [33] M.A. Subirana, L. Paton, J. Hall, A. Brownlow, E.M. Krupp, J. Feldmann, D. Schaumlöffel, Development of mercury analysis by nanosims for the localization of mercury-selenium particles in whale liver, *Anal. Chem.* 93 (37) (2021) 12733–12739.
- [34] I. Strzeminska, C. Factor, J. Jimenez-Lamana, S. Lacomme, M.A. Subirana, P. Le Coustumer, D. Schaumlöffel, P. Robert, J. Szpunar, C. Corot, R. Lobinski, Comprehensive speciation analysis of residual gadolinium in deep cerebellar nuclei in rats repeatedly administered with gadoterate meglumine or gadodiamide, *Invest. Radio.* 57 (5) (2022) 283–292.
- [35] D.M. Runge, T.W. Stock, T. Lehmann, C. Taeye, U. Bernauer, D.B. Stolz, S. Hofmann, H. Foth, Expression of cytochrome P450 2E1 in normal human bronchial epithelial cells and activation by ethanol in culture, *Arch. Toxicol.* 75 (6) (2001) 335–345.
- [36] G.L. Newton, R. Dorian, R.C. Fahey, Analysis of biological thiols: derivatization with monobromobimane and separation by reverse-phase high-performance liquid chromatography, *Anal. Biochem.* 114 (2) (1981) 383–387.
- [37] R.Y. Prasad, S.O. Simmons, M.G. Killius, R.M. Zucker, A.D. Kligerman, C. F. Blackman, R.C. Fry, D.M. Demarini, Cellular interactions and biological responses to titanium dioxide nanoparticles in HepG2 and BEAS-2B cells: role of cell culture media, *Environ. Mol. Mutagen* 55 (4) (2014) 336–342.
- [38] R.Y. Prasad, K. Wallace, K.M. Daniel, A.H. Tennant, R.M. Zucker, J. Strickland, K. Dreher, A.D. Kligerman, C.F. Blackman, D.M. Demarini, Effect of treatment media on the agglomeration of titanium dioxide nanoparticles: impact on genotoxicity, cellular interaction, and cell cycle, *ACS nano* 7 (3) (2013) 1929–1942.
- [39] W. Wu, G. Ichihara, Y. Suzuki, K. Izuoka, S. Oikawa-Tada, J. Chang, K. Sakai, K. Miyazawa, D. Porter, V. Castranova, M. Kawaguchi, S. Ichihara, Dispersion method for safety research on manufactured nanomaterials, *Ind. Health* 52 (1) (2014) 54–65.
- [40] C. Kochar, L. Taneja, P. Kumar Yadav, S.Swarupa Tripathy, Dissolution behaviour of nanoparticles and its usefulness in understanding the toxicity of nanoparticles- a review, *Mater. Today: Proc.* 71 (2022) 254–258.
- [41] J.G. Keller, U.M. Graham, J. Koltermann-Jully, R. Gelein, L. Ma-Hock, R. Landsiedel, M. Wiemann, G. Oberdorster, A. Elder, W. Wohlleben, Predicting dissolution and transformation of inhaled nanoparticles in the lung using abiotic flow cells: The case of barium sulfate, *Sci. Rep.* 10 (1) (2020) 458.
- [42] V. Sokolova, K. Loza, T. Knuschke, J. Heinen-Weiler, H. Jastrow, M. Hasenberg, J. Buer, A.M. Westendorf, M. Gunzer, M. Epple, A systematic electron microscopic study on the uptake of barium sulphate nano-, submicro-, microparticles by bone marrow-derived phagocytosing cells, *Acta Biomater.* 80 (2018) 352–363.
- [43] R.A. Yokel, S. Hussain, S. Garantzios, P. Demokritou, V. Castranova, F.R. Cassee, The Yin: An adverse health perspective of nanoceria: uptake, distribution, accumulation, and mechanisms of its toxicity, *Environ. Sci. Nano* 1 (5) (2014) 406–428.
- [44] R. Lehner, I. Zanoni, A. Banuscher, A.L. Costa, B. Rothen-Rutishauser, Fate of engineered nanomaterials at the human epithelial lung tissue barrier in vitro after single and repeated exposures, *Front. Toxicol.* 4 (2022) 918633.
- [45] A. Nel, T. Xia, L. Mädler, N. Li, Toxic potential of materials at the nanolevel, *Science* 311 (5761) (2006) 622–627.
- [46] R.M. Molina, N.V. Konduru, P.M. Queiroz, B. Figueroa, D. Fu, L. Ma-Hock, S. Groeters, D. Schaudien, J.D. Brain, Fate of barium sulfate nanoparticles deposited in the lungs of rats, *Sci. Rep.* 9 (1) (2019) 8163.
- [47] J. Llop, I. Estrela-Lopis, R.F. Ziolo, A. González, J. Flederermann, M. Dorn, V. G. Vallejo, R. Simon-Vazquez, E. Donath, Z.G. Mao, C.Y. Gao, S.E. Moya, Uptake, biological fate, and toxicity of metal oxide nanoparticles, *Part Part Syst. Char* 31 (1) (2014) 24–35.
- [48] D. Lichtenstein, J. Ebmeyer, T. Meyer, A.C. Behr, C. Kästner, L. Böhmert, S. Juling, B. Niemann, C. Fahrenson, S. Selve, A.F. Thünemann, J. Meijer, I. Estrela-Lopis, A. Braeuning, A. Lampen, It takes more than a coating to get nanoparticles through the intestinal barrier in vitro, *Eur. J. Pharm. Biopharm.* 118 (2017) 21–29.
- [49] H.R. Wirtz, L.G. Dobbs, Calcium mobilization and exocytosis after one mechanical stretch of lung epithelial cells, *Science* 250 (4985) (1990) 1266–1269.
- [50] Q. Zhao, Y. Li, X. Chai, L. Zhang, L. Xu, J. Huang, P. Ning, S. Tian, Interaction of nano carbon particles and anthracene with pulmonary surfactant: the potential hazards of inhaled nanoparticles, *Chemosphere* 215 (2019) 746–752.
- [51] F. Mousseau, J.F. Berret, The role of surface charge in the interaction of nanoparticles with model pulmonary surfactants, *Soft Matter* 14 (28) (2018) 5764–5774.
- [52] T.S. Hauck, A.A. Ghazani, W.C. Chan, Assessing the effect of surface chemistry on gold nanorod uptake, toxicity, and gene expression in mammalian cells, *Small* 4 (1) (2008) 153–159.
- [53] G. Romero, I. Estrela-Lopis, P. Castro-Hartmann, E. Rojas, I. Llarena, D. Sanz, E. Donath, S.E. Moya, Stepwise surface tailoring of carbon nanotubes with polyelectrolyte brushes and lipid layers to control their intracellular distribution and “in vitro” toxicity, *Soft Matter* 7 (15) (2011) 6883–6890.
- [54] A. Mech, K. Rasmussen, P. Jantunen, L. Aicher, M. Alessandrelli, U. Bernauer, E.A. J. Bleeker, J. Bouillard, P. Di Prospero Fanghella, R. Draisci, M. Dusinska, G. Encheva, G. Flament, A. Haase, Y. Handzhiyski, F. Herzberg, J. Huwyler, N. R. Jacobsen, V. Jeliazkova, N. Jeliazkova, P. Nyman, R. Grafström, A.G. Oomen, M. L. Polci, C. Riebeling, J. Sandström, B. Shivachev, S. Stateva, S. Tanasescu, R. Tsekovska, H. Wallin, M.F. Wilks, S. Zellmer, M.D. Apostolova, Insights into possibilities for grouping and read-across for nanomaterials in EU chemicals legislation, *Nanotoxicology* 13 (1) (2019) 119–141.
- [55] M.J. Kustner, D. Eckstein, D. Brauer, P. Mai, J. Hampl, F. Weise, B. Schuhmann, G. Hause, F. Glahn, H. Foth, A. Schober, Modular air-liquid interface aerosol exposure system (MALIES) to study toxicity of nanoparticle aerosols in 3D-cultured A549 cells in vitro, *Arch. Toxicol.* 98 (4) (2024) 1061–1080.